

Electrostatically Driven Nanoballoon Actuator

Hamid Reza Barzegar,^{†,‡,§,||} Aiming Yan,^{†,§,||} Sinisa Coh,^{†,§,⊥} Eduardo Gracia-Espino,[‡] Gabriel Dunn,^{†,§,||} Thomas Wågberg,[‡] Steven G. Louie,^{†,§} Marvin L. Cohen,^{†,§} and Alex Zettl^{*,†,§,||}

[†]Department of Physics, University of California, Berkeley, California 94720, United States

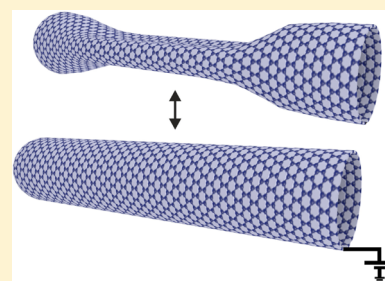
[‡]Department of Physics, Umea University, 90187 Umea, Sweden

[§]Materials Sciences Division, Lawrence Berkeley National Laboratory, Berkeley, California 94720, United States

^{||}Kavli Energy NanoSciences Institute at the University of California, Berkeley and the Lawrence Berkeley National Laboratory, Berkeley, California 94720, United States

Supporting Information

ABSTRACT: We demonstrate an inflatable nanoballoon actuator based on geometrical transitions between the inflated (cylindrical) and collapsed (flattened) forms of a carbon nanotube. In situ transmission electron microscopy experiments employing a nanoelectromechanical manipulator show that a collapsed carbon nanotube can be reinflated by electrically charging the nanotube, thus realizing an electrostatically driven nanoballoon actuator. We find that the tube actuator can be reliably cycled with only modest control voltages (few volts) with no apparent wear or fatigue. A complementary theoretical analysis identifies critical parameters for nanotube nanoballoon actuation.



KEYWORDS: Nanoballoon, actuator, collapsed carbon nanotube, nanomanipulator, reinflation

Inflatable balloon actuators have far-ranging applications. At the macroscale, pneumatically controlled balloon actuators are used to lift buildings after earthquakes, provide impact protection in vehicular collisions (airbags), and enable stents in arterial medical procedures.¹ At the microscale, balloon actuators are employed for aerodynamic control,² micropumps and flow controllers,³ and microbiotic fingers.⁴ Some insect legs are powered by microballoon actuators.⁵ Interestingly, at the nanoscale, balloon actuators are virtually unknown, likely due to the extreme complexity of nanoscale pneumatic control. Recently Shklyav et al.⁶ proposed a charge controlled nanoballoon actuator based on the collapsing and reinflation of a carbon nanotube. Here we employ in situ transmission electron microscopy (TEM) and successfully demonstrate such an electrostatically driven actuator. We present a complementary theoretical analysis and identify critical parameters for nanotube nanoballoon actuation.

Collapsed carbon nanotubes^{7–13} represent an intriguing geometrical configuration intermediate between that of a circular cross-section “inflated” nanotube and a completely flat (multilayer) sharp-edged carbon nanoribbon. The curvature energy of nanotube walls favors an inflated tube, while van der Waals interaction across the innermost wall diameter favors collapse.^{8,14–19} Tubes with low wall number and large diameter are thus highly susceptible to collapse.^{14,20} In the nanoballoon actuator scheme of Shklyav et al.⁶ tubes of appropriate diameter represent a bistable system where external voltages applied to the tubes can, via capacitive effects, render the collapsed and inflated states nearly degenerate with a relatively low activation barrier between them. Other theoretical^{21,22}

studies have investigated thermally driven nanotube state transformation, which is the basis of a thermally driven nanotorsional actuator.²³

In our experiments custom-sized carbon nanotubes with favorable geometry (i.e., for which the collapsed and inflated states are intrinsically relatively close in energy) are initially created in the TEM from a presynthesized large diameter, large wall number carbon nanotube (the “parent” tube), as described below.²⁴ Once such a suitable “daughter” tube is isolated; it spontaneously collapses due to thermal fluctuations or it can be induced to collapse by a small mechanical perturbation (which can be permanently applied). Balloon actuation, i.e., reinflation, is realized by application of a small voltage to the tube, which charges it electrostatically.

The schematic drawings of Figure 1 illustrate the custom nanotube preparation process. Corresponding TEM images from real fabrication experiments are provided in Figure S1. One end of a parent multiwall tube (left side in Figure 1a) is fixed to a copper mesh TEM grid (stationary electrode) via conductive silver paint. The opposite end of the parent tube (right side in Figure 1a) is then in situ spot-welded to a sharp, piezo-controlled, tungsten tip via a bias voltage (typically between 1 to 4 V). Following spot-welding, the tungsten tip moves to the right (Figure 1b), and in doing so it extracts an inner core few-wall “daughter” tube from the parent tube. The daughter tube is then examined for suitability for reversible

Received: June 11, 2016

Revised: October 3, 2016

Published: October 5, 2016

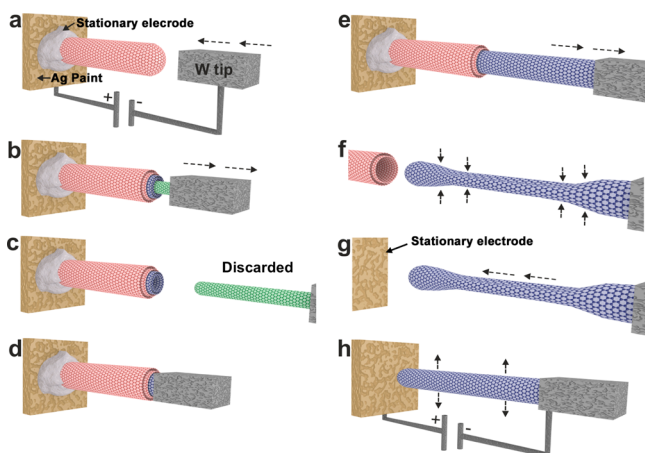


Figure 1. Schematic of method to produce and control custom-sized carbon nanotube for reversible collapse/reinflation. (a) A preformed large-diameter, many-walled nanotube (pink) is affixed to a stationary electrode. (b, c) A mobile tungsten tip burns open and is spot-welded to the tube end and extracts small-diameter core tubes (green) which are later discarded. (d, e) The tungsten tip is then spot-welded to the open end of the chosen daughter tube (blue), and the daughter tube is extracted. (f) The daughter tube is allowed to collapse spontaneously or induced to do so with a small mechanical perturbation. (g, h) The collapsed tube can be reinflated by applying a modest electrical voltage. If the electrical bias is removed, the tube can again collapse, and the reinflation/collapse cycle is repeated. This forms a fatigue-free voltage-controllable nanomechanical actuator.

collapse/reinflation. If this daughter tube is not suitable for the intended experiment (for example, it does not easily collapse because it has too many walls and/or its overall diameter is too small), it is discarded, and a new larger-diameter daughter tube is pulled from the inner region of the parent tube using the same spot-welding and extraction process, as shown in Figures 1d and e. This leads to successively larger overall diameter daughter tubes produced, increasingly susceptible to collapse. The collapsed daughter tube can then be brought into contact with the stationary electrode (Figure 1g) where it can be reinflated via applied external voltage (Figure 1h).

Figure 2 illustrates TEM images from an actual experiment. Figure 2a,b corresponds to the schematic drawings in Figure 1g,h and shows a seven-walled ($n = 7$) tube with an inflated outer diameter of $d = 11.5$ nm (zoomed-out TEM images of the tube in Figure 2a,b are provided in Figure S1f,g). The width of the flattened collapsed part, as determined from the TEM image of Figure 2a, is 16 nm, in accord with the width expected for this tube in the fully collapsed state.²⁵ Both ends of the tube, indicated by circles in Figure 2a, are pinned open (i.e., constrained to maintain a circular cross-section) at all times: the left end by virtue of the intrinsic nanotube hemispherical cap, and the right end via the inflated-state spot-weld to the tungsten nanomanipulator tip. A bias voltage of $V = 3$ V is used to return the tube of Figure 2a to the inflated, cylindrical state (Figure 2b). After removing the bias voltage, the reinflated tube again collapses but can be reinflated in the manner described above, with no apparent wear or fatigue. Indeed, a defect-free, highly flexible tube wall fabric would suggest infinite cycling capability and clearly demonstrates reproducible, nanoballoon actuation. We note that in the examined configuration the tungsten nanomanipulator tip, in addition to supplying variable electrical bias voltage, is also able to impose a small mechanical bias (i.e., perturbation) to the nanotube at all times. This

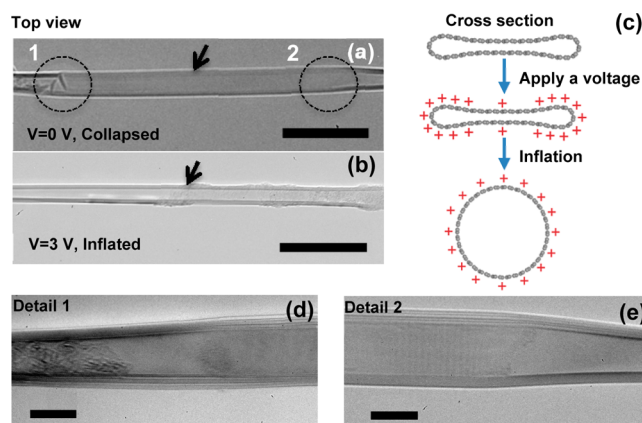


Figure 2. TEM image of: (a) a collapsed tube (with pinned-open ends) and (b) same tube in the inflated state after three cycles of collapse/reinflation. The collapsed portion of the tube in (a) appears wider in this top view. The arrows in a and b mark the same point on the nanotube. (c) Schematic drawings showing the cross section of a nanotube before and after applying voltage as well as the charge distribution for collapsed and reinflated states. (d and e) Zoomed-in TEM images of the left and right pinned-open ends of the collapsed nanotube in part a, with “Detail 1” and “Detail 2” corresponding to the circles 1 and 2 in part a, respectively. Scale bars in a and b are 50 nm; scale bars in d and e are 10 nm.

effectively eliminates the activation barrier between the inflated and collapsed states and prevents hysteresis. The voltage bias thereby becomes a single-valued control parameter.

We now discuss the mechanism for reinflation of a collapsed nanotube. Such a transition requires an external energy that spans the energy difference between two states, and the externally applied voltage plays this key role in reinflation via capacitive effects, as we demonstrate below (the TEM imaging electron beam flux is constant during the experiment and provides only a minor energy offset). The difference in energy per area of an inflated (e_{inflated}) and a collapsed ($e_{\text{collapsed}}$) carbon nanotube can be approximated²⁶ by the following function of the inflated nanotube diameter (d) and number of walls (n):

$$\Delta e = e_{\text{inflated}} - e_{\text{collapsed}} = 2D \frac{n}{d^2} - \left(2.6 \sqrt{DW} \frac{\sqrt{n}}{d} - 0.083 d_0 W \frac{1}{d} - \frac{1}{2} W \right) \quad (1)$$

A positive Δe means that the nanotube prefers a collapsed state, while a negative Δe means that it prefers an inflated state. Here the coefficient D measures the curvature energy of the nanotube. We parametrize D so that the curvature energy density of an inflated single wall nanotube with diameter d equals $2D/d^2$. Taking the average of the density-functional-theory-calculated value of D from refs 27 and 28, we obtain $D = 1.59 \pm 0.09$ eV. Parameter W measures the interaction between opposing faces of the collapsed tube. It is parametrized as a cohesive energy of an infinite graphene bilayer per area of the bilayer. The value of this parameter is not known as accurately as D since it depends somewhat sensitively on the strength of the dispersion forces that are not well-reproduced in a conventional density functional theory calculation. Nevertheless, taking the average value of W from a recent quantum Monte Carlo calculation²⁹ and the value calculated using van der Waals corrected density functional theory,³⁰ we obtain $W = 1.7 \pm 0.3$ eV/nm². Finally, parameter d_0 is the equilibrium

distance between two graphene sheets, which we take equal to 0.333 ± 0.005 nm. Inserting these estimates of D , W , and d_0 into eq 1 yields

$$\Delta e = 3.17 \frac{n}{d^2} - \left(4.24 \frac{\sqrt{n}}{d} - 0.046 \frac{1}{d} - 0.84 \right) \quad [\text{eV/nm}^2] \quad (2)$$

The diameter d is here given in nanometers. The first term in eq 2 is the curvature energy density of the inflated tube. The terms in parentheses account for the curvature energy of the bulged edges of the collapsed tube as well as the cohesive energy of the collapsed region where the opposing faces of the carbon nanotube are in contact.

The left panel of Figure 3 is a contour plot of Δe as a function of n and d . The blue-colored region in Figure 3

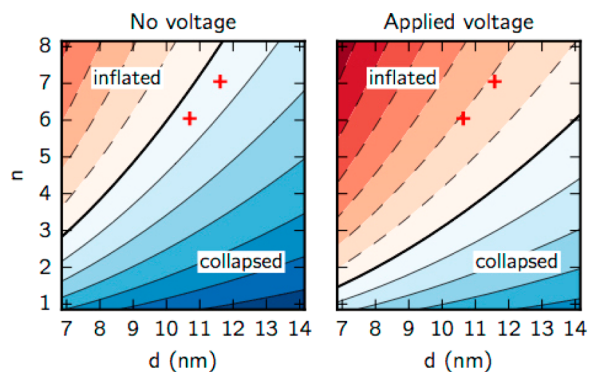


Figure 3. Blue shaded regions indicate the range of tube wall number n and diameter d for which the free energy Δf (see eq 3) is positive, and a collapsed state is preferred over the inflated state. The red region indicates preference for the inflated state, and it is increased when a bias voltage is applied (right panel). The applied voltage is chosen such that $\frac{1}{2}\Delta cV^2$ equals $0.2 \text{ eV/nm}^2 \cdot \text{V}^2$, which here gives $V = 3 \text{ V}$. The experimentally examined tubes are illustrated by cross signs in the figures.

indicates the range of n and d for which Δe is positive indicating that the collapsed state is energetically preferred over the inflated state. Similarly, the red region indicates preference for an inflated state. The thick black line indicates the border between two regions. As expected, nanotubes with a large diameter d and a small number of walls n prefer a collapsed state. This behavior is apparent from eq 2 since the energy density of the inflated tube scales as $\sim n/d^2$, while for the collapsed tube it scales as $\sim n^{0.5}/d$. As explained in more detail

below, the reinflation voltage is not only a function of tube wall number and diameter, but it also depends on the tube capacitance; consequently it is also a function of tube length and electrode configuration. For illustrative purposes in Figure 3, the voltage is chosen so that $\frac{1}{2}\Delta cV^2$ equals $0.2 \text{ eV/nm}^2 \cdot \text{V}^2$, where Δc indicates the difference between tube capacitance in collapse and inflated states. For the reinflatable carbon nanotube described for our experiment ($n = 7$ and $d = 11.5$ nm) we find $\Delta e = 0.04 \pm 0.07 \text{ eV/nm}^2$, indicating that the energies of the collapsed and inflated states are close (with a preferred collapsed state) and thus favorable for collapse/reinflation cycling.

We now incorporate into our model the reinflation control parameter, i.e., the effect of the applied bias voltage V on the nanoballoon actuator state. Adding the energy stored in the electric field between the nanotube and the electrode, as well as the work done to keep the voltage V constant, we obtain the following free energy density difference between the inflated and the collapsed tube:

$$\Delta f = \Delta e - \frac{1}{2}\Delta cV^2 \quad (3)$$

Here $\Delta c = c_{\text{inflated}} - c_{\text{collapsed}}$ is the difference between capacitance per area of an inflated and a collapsed nanotube. The charge distribution on the surface of an inflated nanotube is uniform, while in the collapsed state charge piles up at the bulged ends of the tube (see schematic drawing in Figure 2c). Therefore, the inflated state has a larger capacitance than the collapsed state (i.e., $\Delta c > 0$).

We estimate the magnitude of Δc for a nanotube in our experiment. The voltage V is applied relative to the metallic contact, as shown in Figure 1h. Therefore, the capacitance of the carbon nanotube in this geometry can be approximated by the capacitance of a cylinder (inflated state) or ribbon (collapsed state) with length l and (inflated) diameter d that is oriented perpendicularly to an infinite metallic plane. The distance between the metal contact and the closest end of the cylinder we denote as g . Calculating capacitance in this geometrical setup is analytically intractable, so we compute the capacitance numerically. We solve the Poisson equation using the finite-element method³¹ with boundary conditions that assume perfect metallic screening both in the carbon nanotube and in the contact plane.

Figure 4 shows the calculated Δc as a function of nanotube length (l), inflated diameter (d), and the distance from the metal contact to the end of the carbon nanotube (g). As expected, Δc increases for small l , large d , and small g . From

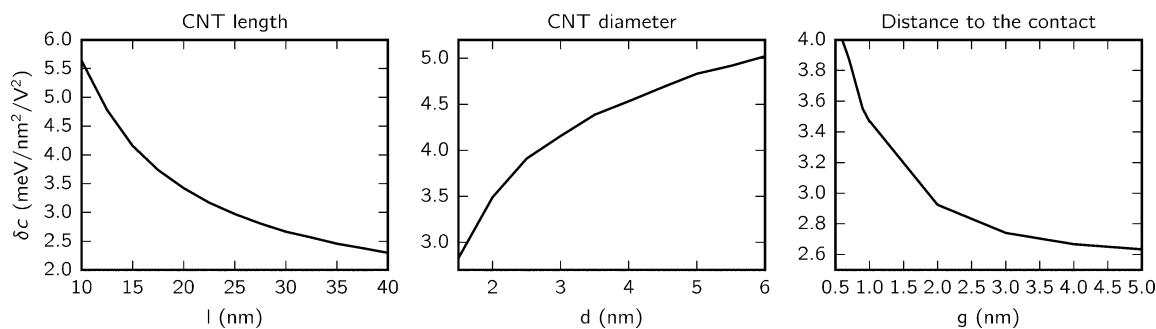


Figure 4. Numerically calculated difference in the capacitance per area of the inflated and the collapsed carbon nanotube as a function of the nanotube length (l), diameter (d), and the distance to the metal contact (g).

these calculations we estimate $\Delta c = 0.004 \text{ eV/nm}^2 \cdot V^2$ for the tube examined in Figure 2a with $l = 250 \text{ nm}$, $d = 11.5 \text{ nm}$, and $g = 0.5 \text{ nm}$. The sign of Δc is positive, as expected from our earlier analysis. We note that, while l and d can be estimated rather easily from our experiment, the magnitude of g is harder to determine. In the limit of large g , we estimate that $\Delta c = 0.002 \text{ eV/nm}^2 \cdot V^2$, which sets a lower bound on Δc . Note that in the opposite limit (small g) the capacitance difference diverges (see the right-most panel of Figure 4).

We now compare our experimentally obtained critical voltage for reinflation with theoretically predicted values. With a kinetic barrier close to zero, the reinflation within our model occurs when the applied voltage V is large enough to change the sign of Δf from positive to negative (see right panel in Figure 3). Using our earlier estimate of Δc and $\Delta \epsilon$ we infer that the critical voltage for reinflation of the CCNT in our experiment lies between 0 and 7 V, consistent with the experimentally determined value of 3 V. The largest source of theoretical error here originates from parameters W and g .

It has been suggested that the change in the free energy of a collapsed tube due to increased temperature may also facilitate the reinflation.^{21,22} Since at high temperatures the inflated state has lower free energy than the collapsed state, Joule heating due to the applied voltage may assist the reinflation process. Applying estimates for current-induced temperature changes and thermal time constants for the experiments at hand, we do not see compelling evidence for thermally driven reinflation.

Finally, we examine details of the pinning constraint. For the experiments described above, both ends of the nanotube remain pinned open at all times (due to hemispherical end-caps or circular cross-section spot-welded ends). Pinning both ends of the tube open slightly raises the energy of the collapsed state and hence further reduces the energy difference between the collapsed and inflated states and facilitates actuator function with modest control voltages. Indeed, with open pinning the inflation process is zipper-like, where the tube inflates via a propagating “inflation wave” originating at the open pinning sites. This is consistent with our model, where a negligible activation barrier is assumed. Pinned open ends of a collapsed tube are apparent from the tapered tube diameters of Figure 2d,e, and similar pinned open ends are strikingly recognizable in side view TEM images as shown in Figure 5a. For the tube of Figure 5a the left side is pinned-open by the “circular” spot-weld to the tungsten tip and the right side is pinned-open by the circular parent tube end (corresponding zoomed-out TEM

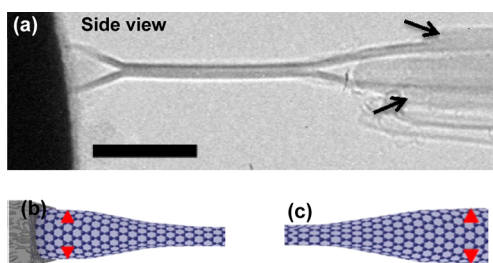


Figure 5. (a) Side-view TEM image of a collapsed tube with pinned-open ends. Arrows on the right side of the tube show the termination of the parent tube, which effectively pins the daughter tube open at that location. Parts b and c are schematic drawings showing the side view of the boundaries between collapsed and inflated parts, corresponding to two ends of the tube. The red triangles indicate the pinned-open ends of the nanotube. Scale bar in part a is 20 nm.

images are provided in Figure S2). Open pinning is schematically illustrated in Figures 5b,c.

To further examine pinning, the end-cap on the left side of the collapsible daughter tube of Figure 2 is burned away in situ via electric discharge. The uncapped carbon nanotube is subsequently found to collapse/reinflated again in a similar manner to that described above. Corresponding TEM images are provided in Figure S3. This suggests that only one pinned-open region along the collapsed tube length is sufficient to initiate the desirable reinflation zipper process.

If the collapsed state has too deep an energy well (e.g., as can occur for a tube with a large diameter and no open pinning), the barrier between the collapsed state and the reinflated state may be too large to be overcome by applying reasonable external voltages. For example, our effort to reinflate a four-walled collapsed tube with an outer diameter of 25 nm was unsuccessful using bias voltages up to 20 V (more examples are provided in Table S1). A small energy difference and small energy barrier between the two states (collapsed and inflated) ensure reasonable voltages for, and cyclability of, the process.

In summary, we experimentally demonstrate a nanotube nanoballoon actuator. The experimental results and complementary theoretical analysis define an approach to identifying critical parameters for nanotube nanoballoon actuation. Our results have implications for nanoscale switches (electronic, optical, thermal), fluid valves and pumps, muscles, grippers, chemical transport, and general nanomatter manipulation.

Methods. The experiment is conducted using a JEOL 2010 TEM operated at 80 keV and a “Nanofactory Instrument AB” nanomanipulator. A photograph of the manipulator TEM holder is provided in Figure S4. The highly crystalline arc-discharge grown MWCNTs are obtained from MER Corporation. A copper mesh TEM grid is cut in half, and the MWCNTs are mounted to its edge by a conductive silver paint. The copper mesh is fixed to a biasing TEM holder by double-sided carbon tape and thereafter connected to the holder circuit by copper wire and silver paint (act as stationary electrode). A sharp tungsten tip with a diameter of few tens of nanometer is prepared by electrochemical etching of tungsten wire in sodium hydroxide solution and is fixed on the movable cap of TEM biasing holder (moveable electrode).

■ ASSOCIATED CONTENT

📄 Supporting Information

The Supporting Information is available free of charge on the ACS Publications website at DOI: 10.1021/acs.nanolett.6b02394.

Additional zoomed-out TEM images of the examined nanotubes, photograph of the experimental setup, and details of the performed experiments (PDF)

■ AUTHOR INFORMATION

✉ Corresponding Author

*E-mail: azettl@berkeley.edu.

📍 Present Address

¹Mechanical Engineering, Materials Science and Engineering, University of California Riverside, Riverside, CA 92521, USA

👤 Author Contributions

H.R.B. and A.Y. contributed equally to this work.

📝 Notes

The authors declare no competing financial interest.

ACKNOWLEDGMENTS

This work was supported in part by the Director, Office of Science, Office of Basic Energy Sciences, Materials Sciences and Engineering Division, of the U.S. Department of Energy under Contract No. DE-AC02-05CH11231, within the Nanomachines Program (KC1203), which provided for TEM characterization and for the continuum model calculation; by the Department of the Navy, Office of Naval Research under Grant No. N00014-16-1-2229 which provided for collapsed nanoribbon synthesis; by the National Science Foundation under grant DMR-1508412 which provided for total energy calculations; and by the Swedish Research Council (grant dnr 2015-00520) which provided support for H.R.B. Computational resources have been provided by the NSF through XSEDE resources at NICS.

REFERENCES

- (1) Kim, D. H.; Lu, N. S.; Ghaffari, R.; Kim, Y. S.; Lee, S. P.; Xu, L. Z.; Wu, J. A.; Kim, R. H.; Song, J. Z.; Liu, Z. J.; Viventi, J.; de Graff, B.; Elolampi, B.; Mansour, M.; Slepian, M. J.; Hwang, S.; Moss, J. D.; Won, S. M.; Huang, Y. G.; Litt, B.; Rogers, J. A. *Nat. Mater.* **2011**, *10* (4), 316–323.
- (2) Grosjean, C.; Lee, G. B.; Hong, W.; Tai, Y. C.; Ho, C. M. *Micro Electro Mechanical Systems - Ieee Eleventh Annual International Workshop Proceedings* **1998**, 166–171.
- (3) Jeong, O. C.; Konishi, S. *Sens. Actuators, A* **2007**, *135* (2), 849–856.
- (4) Lu, Y. W.; Kim, C. J. *Boston Transducers'03: Digest of Technical Papers, Vols 1 and 2*; **2003**; pp 276–279.
- (5) Parry, D. A.; Brown, R. H. *J. Exp. Biol.* **1959**, *36* (2), 423–433.
- (6) Shklyav, O. E.; Mockensturm, E.; Crespi, V. H. *Phys. Rev. Lett.* **2011**, *106* (15), 155501.
- (7) Chopra, N. G.; Benedict, L. X.; Crespi, V. H.; Cohen, M. L.; Louie, S. G.; Zettl, A. *Nature* **1995**, *377* (6545), 135–138.
- (8) Zhang, C. G.; Bets, K.; Lee, S. S.; Sun, Z. Z.; Mirri, F.; Colvin, V. L.; Yakobson, B. I.; Tour, J. M.; Hauge, R. H. *ACS Nano* **2012**, *6* (7), 6023–6032.
- (9) Li, Y. F. *Phys. Chem. Chem. Phys.* **2014**, *16* (5), 1921–1929.
- (10) Zhong, X. H.; Wang, R.; Liu, L. B.; Kang, M.; Wen, Y. Y.; Hou, F.; Feng, J. M.; Li, Y. L. *Nanotechnology* **2012**, *23* (50), S05712.
- (11) Choi, D. H.; Wang, Q.; Azuma, Y.; Majima, Y.; Warner, J. H.; Miyata, Y.; Shinohara, H.; Kitaura, R. *Sci. Rep.* **2013**, *3*, 1617.
- (12) Crespi, V. H.; Chopra, N. G.; Cohen, M. L.; Zettl, A.; Louie, S. G. *Phys. Rev. B: Condens. Matter Mater. Phys.* **1996**, *54* (8), 5927–5931.
- (13) Yu, M. F.; Dyer, M. J.; Chen, J.; Qian, D.; Liu, W. K.; Ruoff, R. S. *Phys. Rev. B: Condens. Matter Mater. Phys.* **2001**, *64* (24), 241403.
- (14) Benedict, L. X.; Chopra, N. G.; Cohen, M. L.; Zettl, A.; Louie, S. G.; Crespi, V. H. *Chem. Phys. Lett.* **1998**, *286* (5–6), 490–496.
- (15) Zhang, S.; Khare, R.; Belytschko, T.; Hsia, K. J.; Mielke, S. L.; Schatz, G. C. *Phys. Rev. B: Condens. Matter Mater. Phys.* **2006**, *73* (7), 075423.
- (16) Liu, H. J.; Cho, K. J. *Appl. Phys. Lett.* **2004**, *85* (5), 807–809.
- (17) Wang, Q.; Kitaura, R.; Yamamoto, Y.; Arai, S.; Shinohara, H. *Nano Res.* **2014**, *7* (12), 1843–1848.
- (18) Xiao, J.; Liu, B.; Huang, Y.; Zuo, J.; Hwang, K. C.; Yu, M. F. *Nanotechnology* **2007**, *18* (39), 395703.
- (19) He, M.; Dong, J.; Zhang, K.; Ding, F.; Jiang, H.; Loiseau, A.; Lehtonen, J.; Kauppinen, E. I. *ACS Nano* **2014**, *8* (9), 9657–9663.
- (20) Elliott, J. A.; Sandler, J. K. W.; Windle, A. H.; Young, R. J.; Shaffer, M. S. P. *Phys. Rev. Lett.* **2004**, *92* (9), 095501.
- (21) Chang, T. *Phys. Rev. Lett.* **2008**, *101* (17), 175501.
- (22) Chang, T.; Guo, Z. *Nano Lett.* **2010**, *10* (9), 3490–3493.
- (23) Senga, R.; Hirahara, K.; Nakayama, Y. *Appl. Phys. Lett.* **2012**, *100* (8), 083110.
- (24) Cumings, J.; Zettl, A. *Science* **2000**, *289* (5479), 602–604.
- (25) Barzegar, H. R.; Gracia-Espino, E.; Yan, A.; Ojeda-Aristizabal, C.; Dunn, G.; Wågberg, T.; Zettl, A. *Nano Lett.* **2015**, *15* (2), 829–834.
- (26) Tang, T.; Jagota, A.; Hui, C.-Y.; Glassmaker, N. J. *J. Appl. Phys.* **2005**, *97* (7), 074310.
- (27) Sanchez-Portal, D.; Artacho, E.; Soler, J. M.; Rubio, A.; Ordejon, P. *Phys. Rev. B: Condens. Matter Mater. Phys.* **1999**, *59* (19), 12678–12688.
- (28) Gulseren, O.; Yildirim, T.; Ciraci, S. *Phys. Rev. B: Condens. Matter Mater. Phys.* **2002**, *65* (15), 153405.
- (29) Mostaani, E.; Drummond, N. D.; Fal'ko, V. I. *Phys. Rev. Lett.* **2015**, *115* (11), 115501.
- (30) Hamada, I.; Otani, M. *Phys. Rev. B: Condens. Matter Mater. Phys.* **2010**, *82* (15), 153412.
- (31) Hecht, F. *J. Numer. Math.* **2012**, *20* (3–4), 251–265.